Rev. Roum. Sci. Techn.– Électrotechn. et Énerg.
Vol. **71**, *4*, pp. 507–512, Bucarest, 2026

PHYSICS-INFORMED NEURAL NETWORK-BASED SENSORLESS SPEED ESTIMATION OF BRUSHLESS DIRECT CURRENT MOTOR DRIVE

PRIYANKA SASIDHARAN[1], SRIRANJANI RAMAKRISHNAN[2], JAYALALITHA SUBBAIAH[3]

Keywords: Sensorless control; Brushless direct current (BLDC) motor; Extended Kalman filter; Electric vehicle; Physics-informed neural network (PINN).

Brushless direct current (BLDC) motors are employed for electric vehicles (EVs), medical equipment, and military robots because of their fast dynamic speed response and wide range of speed regulation characteristics. However, conventional methods are not suitable for dynamic speed-varying conditions, which leads to parameter variation issues and longer computational time. Therefore, in this article, a novel Extended Kalman Filter (EKF) for sensorless speed detection of a BLDC motor is implemented using a machine learning-based physics-informed neural network (PINN) algorithm. Variables obtained from the PINN training are incorporated into the novel EKF; then, with the implemented model, the BLDC motor speed tracks the reference speed in dynamic, speed-varying conditions, thereby eliminating parameter variation issues and achieving shorter computational time as well. The implemented sensorless speed estimation scheme is compared with the conventional algorithms, and the results are presented using LAUNCHXL-F28379D. Also, compared with other conventional sensorless speed estimation techniques, the implemented method achieved reduced speed errors of 0.003% and 0.03% at 1500 rpm and 2000 rpm, respectively.

1. INTRODUCTION

Electric vehicles have become the primary research focus due to their pollution-free nature, higher energy efficiency, and lower maintenance. Primary propulsion in EV is provided by the BLDC motor. BLDC motor has the advantage of mounting the rotor inside the stator, thereby achieving a wider cross-sectional area for the armature winding, and heat conduction through the BLDC motor frame is improved. Therefore, electrical loading is increased, which results in higher specific torque. Higher efficiency is possible than that of other commutator motors of equivalent size. Also, the BLDC motor has no mechanical commutator like a brushed DC motor; instead, electronic switching is provided by an inverter. The exact position of the rotor is needed for proper BLDC motor commutation. Rotor position is determined from external Hall-Effect sensors. Sensors are erected at 60° electrical intervals, and they are aligned with the stator winding. Three Hall-Effect sensors are mounted to predict six rotor positions. However, one of the costlier components in a BLDC motor is the Hall-effect sensor, which induces thermal sensitivity issues, harmonics, noise, and vibration into the BLDC motor system. Thus, elimination of the Hall-effect sensor reduces the complexity of construction of the BLDC motor. Sensorless control of a BLDC motor refers to the estimation of motor speed without relying on Hall-Effect sensors, hence decreasing the motor cost, increasing reliability, and thereby improving the efficiency of the motor. Thus, the sensorless speed control methods are discussed as follows.

Instantaneous phase inductance is varied for determining the BLDC motor's rotor position. This is achieved by estimating the unknown phase inductance using an inductance bridge. Thus, drawbacks associated with the mutual inductance effect and accuracy degradation due to changes in sampling rate are overcome [1]. An artificial neural network (ANN) based method uses voltage and current information for estimating the speed and rotor position of a BLDC motor. Estimation accuracy is improved at low-speed operating conditions. ANN achieves robustness against load disturbances and parameter variations [2]. Pulse Amplitude Modulation (PAM) method with a DC-link current sensor is implemented for detecting the rotor position. During the entire operating speed range, back-EMF is detected accurately. A commutation technique is introduced to achieve reliability and smoother torque operation [3]. The virtual third harmonic method is used to improve the accuracy of rotor position estimation, which reduces the sensitivity of the estimation process under parameter variation conditions. Accurate commutation is ensured with a robust control technique [4]. Variable slope Sliding Mode Observer (SMO) is used for detecting back-EMF and rotor position of BLDC motor [5–8]. However, the above-mentioned methods suffer from chattering and high-frequency harmonics.

A combination of adaptive delay signal cancellation (ADSC) and synchronous reference frame Phase Locked Loop (PLL) is employed for detecting the rotor position and speed of a BLDC motor even during low-speed operating conditions [9]. An improved dual second-order generalized integrator (DSOGI-PLL) observer is used for detecting the rotor position and speed of a BLDC motor, thereby reducing the commutation error. Harmonic rejection and signal filtering are improved by the DSO-GI observer, while accurate phase synchronization is ensured by the phase-locked loop (PLL) [10]. A comprehensive review of various methods for sensorless control of BLDC motor drives is discussed. The back-EMF method has lower performance at low speeds, whereas SMO, EKF, and MRAS are suitable for wide speed ranges but involve computational complexity in the BLDC motor system [11]. However, the above-mentioned methods are sensitive to measurement noise, have high power consumption, and have lower harmonic attenuation.

The field-oriented control (FOC) method is implemented for rotor position estimation of a BLDC motor. FOC makes the current vector align with the rotor flux for optimal torque production, thus improving the dynamic performance and efficiency of the motor [12]. A novel EKF is used to estimate three-phase back-EMF and stator current, whereas the speed of the BLDC motor is detected with machine learning algorithms like ANN, random forest (RF), and k-nearest neighbor (k-NN) [13]. A model predictive control (MPC) observer is implemented for determining the rotor position and speed of the BLDC motor. MPC dynamically adjusts the voltage vector to reduce iron loss, because conventional BLDC motors face limitations due to iron loss at high speeds

[1,2,3] SASTRA Deemed to be University, Thirumalaisamudram, Thanjavur, Tamil Nadu 613401, India.
E-mails: dpfi0423011676@sastra.ac.in, mathusri@eee.sastra.edu (correspondence), sj_instru@eie.sastra.edu

DOI: 10.59277/RRST-EE.2026.4.5

and rapidly varying load conditions [14]. A lower-order disturbance rejection control strategy combined with an observer-based technique is used for sensorless speed control. Terminal voltage is used for estimating the BLDC motor's rotor position [15]. However, these methods involve higher computational load, tuning difficulties, and steady-state error.

A solar photovoltaic (PV) panel is integrated with the e-rickshaw powertrain to reduce the need for grid charging. Back-EMF zero-crossing point detection with adaptive correction is used for detecting rotor position. Due to asymmetric machine parameters, zero-crossing point timing shifts, and resistance tolerance in the detection circuit, back-EMF amplitude shifts occur, resulting in commutation error. A phase-dependent threshold is adjusted so that the asymmetry in machine parameters is compensated, and by adjusting the common bias of the threshold, the resistance tolerance effect is canceled [16]. Fuzzy-logic direct torque control (DTC) is implemented for a five-leg inverter to independently control two induction motors using a single converter. Thus, reducing hardware complexity and cost [17]. Hybrid intelligent control frameworks are implemented, which significantly enhance the performance and efficiency in complex electromechanical and industrial systems. Also, with EKF, it achieves better stability, faster transients, and higher energy efficiency in EV power trains, synchronous machines, and industrial heat exchangers [18–22]. However, these methods suffer from instability and lower accuracy.

To overcome the above-mentioned issues, a novel EKF is implemented for sensorless speed estimation of a BLDC motor with a machine learning-based PINN algorithm. It uses a six-step metal-oxide-semiconductor field-effect transistor (MOSFET) switch, shown in Fig. 1, and compares conventional methods in Table 1. The primary focus of this research article is a novel EKF that estimates the BLDC motor speed with reduced speed error under high-speed operating conditions.

The novel contribution of this article is given by,

1. Development of a novel EKF with a PINN algorithm for continuous speed estimation of a BLDC motor.
2. This work embeds BLDC motor physics directly into a data-driven neural network algorithm for achieving improved speed estimation accuracy.
3. The novel EKF state is updated using trained PINN variables to reduce sensitivity to parameter variation conditions.
4. Speed tracking is accurate for all the operating speed range, including zero-speed start-up condition.
5. Convergence is faster than the conventional ANN algorithm and achieves shorter computational time.

2. CONVENTIONAL SENSORLESS SPEED ESTIMATION ALGORITHMS

2.1 TERMINAL VOLTAGE SENSING ALGORITHM

Upon estimating the terminal voltage of the non-excited phase winding, motor speed is detected. Commutation of a BLDC motor is controlled accurately with the terminal voltage sensing algorithm. BLDC motor equation is given by

$$v_{\mathrm{AG}} = R_s i_{\mathrm{A1}} + (L_s - M_s)\frac{\mathrm{d}i_{\mathrm{A}}}{\mathrm{d}t} + e_{\mathrm{A1}} + V_N, \quad (1)$$

$$v_{\mathrm{BG}} = R_s i_{\mathrm{B1}} + (L_s - M_s)\frac{\mathrm{d}i_{\mathrm{B}}}{\mathrm{d}t} + e_{\mathrm{B1}} + V_N, \quad (2)$$

$$v_{\mathrm{CG}} = \mathrm{R_s} i_{\mathrm{C1}} + (\mathrm{L_s} - \mathrm{M_s})\frac{\mathrm{d}i_{\mathrm{C}}}{\mathrm{d}t} + e_{\mathrm{C1}} + V_N, \quad (3)$$

where v_{AG}, v_{BG}, v_{CG} and i_{A1}, i_{B1}, i_{C1} are three-phase voltages and currents of the BLDC motor. R_S,L_sL_S, and M_S are the stator resistance, self-inductance, and mutual inductance of each winding. e_{A1}, e_{B1} and e_{C1} denote the back-EMF signals for the three phases. Also, V_N is the neutral point voltage. The terminal voltage sensing algorithm operates when phase A and phase B are energized, and phase C is not energized.

$$e_{\mathrm{A1}} + e_{\mathrm{B1}} = 0, \quad (4)$$

$$i_{\mathrm{A1}} + i_{\mathrm{B1}} = 0. \quad (5)$$

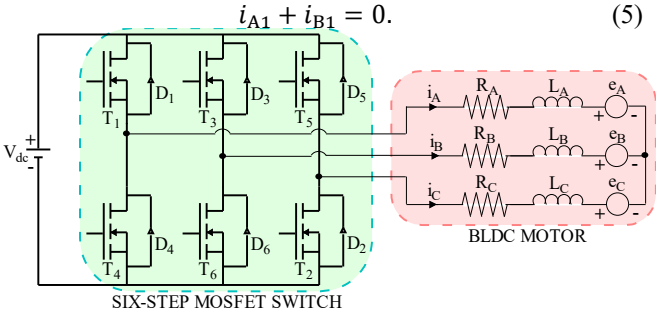


Fig. 1 – Schematic of BLDC motor with six-step MOSFET switch.

Table 1

Comparison among sensorless techniques.

Sensorless Techniques	Advantages	Dis-advantages
Inductance variation [1]	• Estimation is not affected by load torque variation. • Reliability issues and cost are reduced significantly. • Accuracy is independent of the sampling frequency change.	• Estimation accuracy degrades at high-speed operating condition. • Requires additional hardware. • Switching transients and Pulse Width Modulation (PWM) noise affects the actual signals.
Artificial NN (ANN) [2]	• ANN learns from the phase voltage terminals, so this is independent of motor parameters. • Zero crossing detection error, delays in filters and sensitivity to noise in conventional back-EMF are overcome with ANN.	• Needs external encoder to train ANN, which leads to increasing the complexity of hardware. • Performance degrades at standstill operating condition. • Accuracy of speed estimation is lesser during low-speed.
Adaptive SMO [5]	• Speed tracking is continuous. • Independent of parameter variation condition.	• More sensitive to sliding surface and feedback gain. • Both current sensing and voltage sensing are required.
Variable slope SMO [6]	• Parameter sensitivity is lesser compared to other model-based methods. • Converges faster at high-speed operating condition.	• Performance degrades at low-speed operating condition. • Tuning of the slope increases the complexity of hardware design.
DSOGI-PLL [10]	• Harmonics is reduced and phase delay is avoided thereby improving the accuracy of commutation. • Robust dynamic performance under sudden speed and load variation conditions.	• Higher computational burden. • Complexity arises while tuning the parameter for DSOGI gain and PLL bandwidth.
EKF [13], [22]	• Dynamic performance is improved. • Lower cost and higher reliability. • Freewheeling current distortion and neutral point noise are reduced.	• Estimation accuracy is lower at low-speed operating condition. • Tuning of EKF is complex. • Better dynamic performance under sudden load and speed varying conditions.
Novel EKF	• Complexity in tuning the EKF algorithm is overcome. • Reduced speed error is achieved without any additional hardware.	• Performance depends completely on the training dataset. • Sensitive to measurement noise.

	• Wide speed range operation is possible. • Computational burden is less.	

$$v_{\mathrm{AG}} + v_{\mathrm{BG}} = R_s(i_{A1} + i_{\mathrm{B1}}) + (L_s - M_s)\left(\frac{\mathrm{d}i_{\mathrm{A1}}}{\mathrm{d}t} + \frac{\mathrm{d}i_{\mathrm{B1}}}{\mathrm{d}t}\right) + (e_{\mathrm{A1}} + \mathrm{e}_{\mathrm{B1}}) + 2V_N. \quad (6)$$

Substituting (4) and (5) into (6) results in

$$V_N = \frac{v_{\mathrm{AG}}+v_{\mathrm{BG}}}{2}, \quad (7)$$

From (1), (2) and (3)

$$e_{\mathrm{C1}} = v_{\mathrm{CG}} - \frac{v_{\mathrm{AG}}+v_{\mathrm{BG}}}{2}. \quad (8)$$

Equation (8) describes the condition when phases A and B are energized, and phase C is not energized. Similarly, for the other phases, it is given by

$$e_{\mathrm{B1}} = v_{\mathrm{BG}} - \frac{v_{\mathrm{AG}}+v_{\mathrm{CG}}}{2}, \quad (9)$$

$$e_{\mathrm{A1}} = v_{\mathrm{AG}} - \frac{v_{\mathrm{BG}}+v_{\mathrm{CG}}}{2}. \quad (10)$$

Table 2

Motor parameters.

Parameter	Unit	Value
DC-link voltage	V	500
Stator phase resistance	W	0.5
Stator phase inductance	H	0.001
Flux linkage	Weber	0.175
Inertia	kg.m2	0.01
Viscous damping	N.m.s	0.001
Pole pairs	-	4
Rated Torque	Nm	2
Number of poles	-	8

2.2 BACK-EMF ALGORITHM

Back-EMF zero-crossing is estimated and divided into 30° electrical angles for determining rotor position information and speed of the BLDC motor. In the case of BLDC motor drives with variable speed control, the occurrence of commutation instants in the winding leads to inaccuracy in sensorless speed control. However, this drawback is overcome with the line back-EMF algorithm because it eliminates the determination of the phase-shifting angle. The zero-crossing point of the line back-EMF is implemented for detecting commutation instants of the winding. Thus, commutation accuracy in speed control is improved.

$$\frac{\mathrm{d}i_{\mathrm{A}}}{\mathrm{d}t} = \frac{i_{\mathrm{A1}}-i_{\mathrm{A,prev}}}{\mathrm{T_s}}, \quad (11)$$

where $i_{\mathrm{A,prev}}$ is the previous sample of the phase A stator current and $\mathrm{T_s}$ is the sampling time.

$$\mathrm{e_{A1}} = v_{\mathrm{AG}} - R_s i_{\mathrm{A}} - \frac{L_s(i_{\mathrm{A1}}-i_{\mathrm{A1,prev}})}{\mathrm{T_s}}. \quad (12)$$

2.3 EXTENDED KALMAN FILTER ALGORITHM

EKF is used to determine the rotor position and speed of a BLDC motor. EKF is a full-order observer for recurrent state estimation for a dynamic system that is non-linear in real time. The observer uses the machine terminal voltage and current to estimate the BLDC motor speed, thereby eliminating the need for external Hall-Effect sensors. Non-linear functions are linearized by EKF using Taylor series expansion. EKF employs a state transition function that is non-linear for predicting the next state from the current estimated state. A non-linear measurement function is applied to the predicted state to determine the expected measurement. However, the speed estimation accuracy of the EKF algorithm becomes lower during low-speed operating conditions because of variations in machine parameters and low-voltage signal measurement inaccuracies.

3. NOVEL EXTENDED KALMAN FILTER ALGORITHM WITH MACHINE LEARNING-BASED PINN ALGORITHM

Implementation of the novel EKF is given in Fig. 2, whereas the representation of stator frame voltage equations with respect to stator flux linkage is

$$v_{\mathrm{ds}} = R_s i_{\mathrm{ds}} + \frac{\mathrm{d}}{\mathrm{d}t}(\varphi_{\mathrm{ds}}), \quad (13)$$

$$v_{\mathrm{qs}} = R_s i_{\mathrm{qs}} + \frac{\mathrm{d}}{\mathrm{d}t}(\varphi_{\mathrm{qs}}), \quad (14)$$

where v_{ds}, v_{qs}, i_{ds}, i_{qs}, φ_{ds} and φ_{qs} are d-q component voltage, current, and flux linkage.

$$\bar{\varphi}_{\mathrm{s}} = L_s \bar{\mathrm{I}}_{\mathrm{s}} + \bar{\varphi}_{\mathrm{f}}, \quad (15)$$

where $\bar{\varphi}_{\mathrm{s}}$ and $\bar{\varphi}_{\mathrm{f}}$ are stator and rotor flux linkages, L_s is synchronous inductance, and $\bar{\mathrm{I}}_{\mathrm{s}}$ is reference stator current. Reconstruction of (15) into d-q components is given by

$$\varphi_{\mathrm{ds}} = L_s i_{\mathrm{ds}} + \hat{\varphi}_{\mathrm{f}}\cos\vartheta_{\mathrm{e}}, \quad (16)$$

$$\varphi_{\mathrm{qs}} = L_s i_{\mathrm{qs}} + \hat{\varphi}_{\mathrm{f}}\sin\vartheta_{\mathrm{e}}, \quad (17)$$

where $\hat{\varphi}_{\mathrm{f}}$ is the estimated flux linkage, $\cos\vartheta_{\mathrm{e}}$ and $\sin\vartheta_{\mathrm{e}}$ are the electrical rotor angles. Differentiating (16) and (17) and substituting into (13) and (14) yields

$$v_{\mathrm{ds}} = R_s i_{\mathrm{ds}} + L_s \frac{\mathrm{d}}{\mathrm{d}t}(i_{\mathrm{ds}}) - \hat{\varphi}_{\mathrm{f}}\omega_{\mathrm{e}}\sin\vartheta_{\mathrm{e}}, \quad (18)$$

$$v_{\mathrm{qs}} = R_s i_{\mathrm{qs}} + L_s \frac{\mathrm{d}}{\mathrm{d}t}(i_{\mathrm{qs}}) - \hat{\varphi}_{\mathrm{f}}\omega_{\mathrm{e}}\cos\vartheta_{\mathrm{e}}. \quad (19)$$

The state variable form of the dynamic machine model is represented as

$$\frac{\mathrm{d}\mathbf{X}}{\mathrm{d}t} = \mathbf{f}(\bar{\mathbf{X}}) = \mathbf{B}\bar{\mathbf{U}}, \quad (20)$$

where $\bar{\mathbf{X}} = [i_{\mathrm{ds}} \quad i_{\mathrm{qs}} \quad \omega_{\mathrm{e}} \quad \vartheta_{\mathrm{e}}]^{\mathrm{T}}$ is the state vector, $\bar{\mathbf{U}} = [v_{\mathrm{ds}} \quad v_{\mathrm{qs}}]^{\mathrm{T}}$ is the input vector, $\mathbf{Y} = [i_{\mathrm{ds}} \quad i_{\mathrm{qs}}]^{\mathrm{T}}$ is the output vector, whereas **B** and **C** are the input matrix and output matrix.

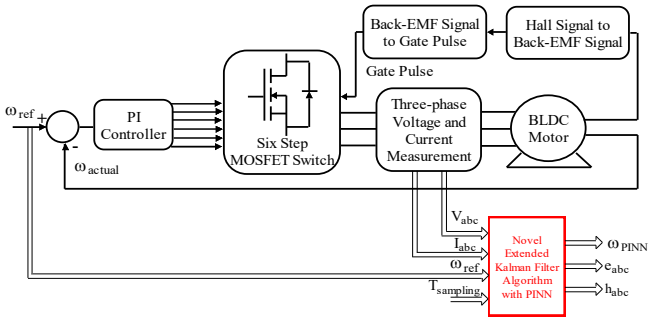


Fig. 2 – Block diagram representation of sensorless speed estimation of a BLDC motor with a novel EKF-based PINN algorithm.

$$\mathbf{f}(\bar{\mathbf{X}}) = \begin{bmatrix} -\frac{R_s}{L_s} i_{\mathrm{ds}} + \frac{\hat{\varphi}_{\mathrm{f}}}{L_s}\omega_{\mathrm{e}}\sin\vartheta_{\mathrm{e}} \\ -\frac{R_s}{L_s} \mathrm{i_{qs}} + \frac{\hat{\varphi}_{\mathrm{f}}}{L_s}\omega_{\mathrm{e}}\cos\vartheta_{\mathrm{e}} \\ 0 \\ \omega_{\mathrm{e}} \end{bmatrix}, \quad (22)$$

$$\mathbf{B} = \begin{bmatrix} \frac{1}{L_s} & 0 \\ 0 & \frac{1}{L_s} \\ 0 & 0 \\ 0 & 0 \end{bmatrix}, \quad (23)$$

$$\mathbf{C} = \begin{bmatrix} 1 & 0 & 0 & 0 \\ 0 & 1 & 0 & 0 \end{bmatrix}. \quad (24)$$

PINN algorithm is implemented using a fully connected feed-forward neural network consisting of three layers and two hidden layers followed by one output layer. The forward propagation through the network is given by

$$\bar{\mathbf{a}}_1 = \tanh(\mathbf{W}_1\bar{\mathbf{x}} + \bar{\mathbf{b}}_1), \quad (25)$$

$$\bar{\mathbf{a}}_2 = \tanh(\mathbf{W}_2\mathbf{a}_1 + \mathbf{b}_2), \quad (26)$$

$$\bar{\mathbf{z}}_3 = \mathbf{W}_3\bar{\mathbf{a}}_2 + \bar{\mathbf{b}}_3 \quad (27)$$

where $\bar{\mathbf{x}}$ denotes the input vector, $\mathbf{W}_1$, $\mathbf{W}_2$, $\mathbf{W}_3$ represent the weight matrices, $\bar{\mathbf{b}}_1$, $\bar{\mathbf{b}}_2$, $\bar{\mathbf{b}}_3$ represent the bias vectors, and $\bar{\mathbf{a}}_1$ and $\bar{\mathbf{a}}_2$ denote the activation outputs of the two hidden layers. The NN output $\bar{\mathbf{z}}_3$ provides the normalized speed estimation, which is subsequently converted into the predicted motor speed. The predicted speed is then used in the EKF prediction stage to update the motor state variables,

$$\omega_{est} = \bar{\mathbf{z}}_3(1)\omega \quad (28)$$

where $\bar{\mathbf{z}}_3(1)$ is normalized speed estimation, ω_{est} and ω are the estimated and reference speeds of the BLDC motor,

$$\omega_{pred} = k(\alpha\omega + (1-\alpha)\omega_{est} + u), \quad (29)$$

where ω_{pred} is the predicted speed, k is constant, α is the weighting factor, and u is the correction factor,

$$\theta_{pred} = \theta(k+1) = \text{mod}\, 2\pi\,(\theta(k) + \omega_{pred}T_s), \quad (30)$$

$$e_{a_{pred}} = \omega_{pred}\text{trapEMF}(\theta_{pred}), \quad (31)$$

$$e_{b_{pred}} = \omega_{pred}\text{trapEMF}(\theta_{pred} - 120^{\circ}), \quad (32)$$

$$e_{c_{pred}} = \omega_{pred}\text{trapEMF}(\theta_{pred} + 120^{\circ}), \quad (33)$$

where $e_{a_{pred}}$, $e_{b_{pred}}$ and $e_{c_{pred}}$ are the three-phase predicted back-EMF signals and θ_{pred} is the predicted rotor angle.

The data loss (L_{data}) is given by

$$L_{data} = \frac{1}{N}\sum_{k=1}^{N}\left(\omega_m^{NN}(k) - \omega_m(k)\right)^2, \quad (34)$$

where N is the total number of training samples; $\omega_m^{NN}(k)$ is the motor speed estimated by the neural network; $\omega_m(k)$ is the reference speed of the motor. Total loss (L_{total}) becomes

$$L_{total} = L_{data} + \lambda L_{physics}, \quad (35)$$

where L_{data} is the loss due to the estimated speed and actual motor speed; $L_{physics}$ is the physics-based loss term; and λ is the weighting factor. Weight update during backpropagation is given by

$$W \leftarrow W - \eta\frac{\delta L_{total}}{\delta W}, \quad (36)$$

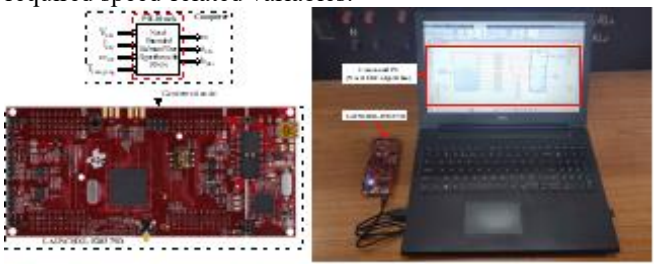
where W is the neural-network weights and η is the learning rate. Also, the gradient of the total loss is given by

$$\frac{\delta L_{total}}{\delta W} = \frac{\delta L_{data}}{\delta W} + \lambda\frac{\delta L_{physics}}{\delta W}. \quad (37)$$

3. EXPERIMENTAL VALIDATION AND ANALYSIS

BLDC motor parameters are given in Table 2. Simulink model, hardware incorporation, and its results are illustrated in Figs. 3 to7, representing the Simulink model, training results, and confusion matrix. At lower speeds, the back-EMF magnitude is relatively small, resulting in weaker electrical information available for accurate sensorless speed estimation. Consequently, the voltage and current signals contain less distinctive speed-related information, and the EKF correction becomes more sensitive to modeling errors and signal variations. As the motor speed increases, the back-EMF magnitude and the corresponding electrical information increase, allowing the PINN to provide more effective state correction and resulting in significantly lower speed-estimation error. Tables 3 to 9 show performance metrics.

The implemented algorithm is validated using a processor-in-the-loop (PIL) implementation. Here, the TI LAUNCHXL-F28379D C2000 controller constitutes the hardware platform, while the BLDC motor drive, inverter, motor electrical model, sensing signals, and control algorithm are implemented in the MATLAB/Simulink environment. The generated code of the EKF algorithm is deployed and executed on the C2000 controller through the PIL interface. The Simulink model supplies the required input signals to the embedded algorithm, and the estimated speed obtained from the C2000 implementation is returned to the Simulink environment for validation. Hence, the reported results represent hardware-based execution of the implemented algorithm through PIL. In the implemented EKF algorithm, the PINN training process is performed prior to real-time implementation. During online operation, the trained network performs only a forward pass to obtain the required speed-related variables.



(a) (b)

Fig. 3 – (a) Visual representation of interfacing the PIL block into hardware and (b) Experimental platform of the novel EKF algorithm with the machine learning-based PINN algorithm.

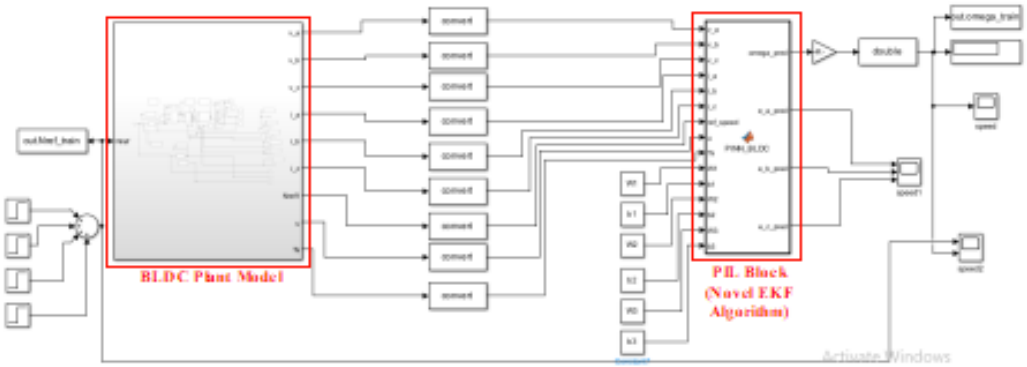


Fig. 4 – Simulink model of the implemented novel EKF with the PINN algorithm.

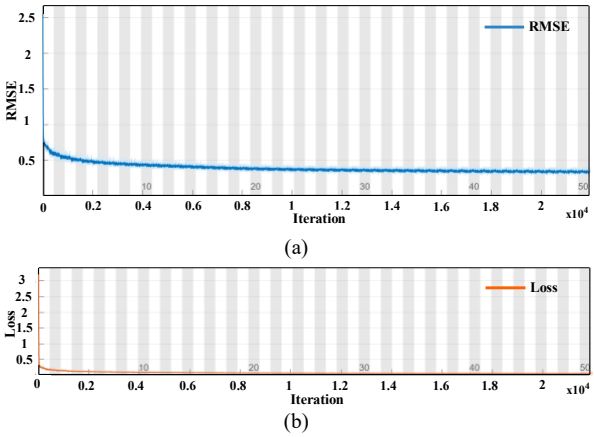


Fig. 5 – Results of training the machine learning-based PINN algorithm for determining (a) RMSE and (b) Loss.

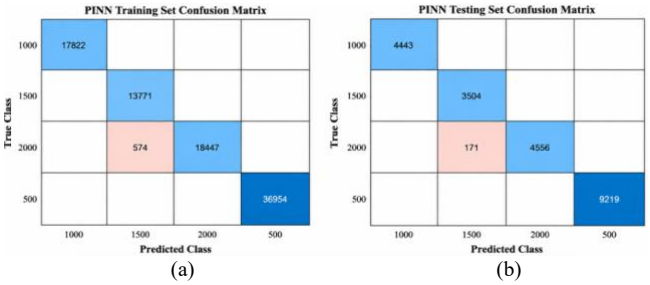


Fig. 6 – Confusion matrix of PINN for (a) Training and (b) Testing.

Table 3

Performance evaluation of the PINN for BLDC motor speed estimation.

Performance metric	Training set	Testing set
Number of samples	87568	21893
PINN accuracy	95.2775%	95.2721%
Train and test accuracy	99.3445%	99.2189%
MAPE	4.7225%	4.7279%
F1 score	0.9894	

Table 4

Comparison among conventional sensorless speed estimation algorithms.

Speed (rpm)	Speed error (%)			
	Terminal voltage sensing algorithm	Back-EMF algorithm	EKF algorithm	Novel EKF with PINN algorithm
500	0.08	0.08	0.3	0.2
1000	0.12	0.12	0.003	0.04
1500	0.18	0.18	0.16	0.003
2000	0.21	0.21	0.10	0.03

Table 5

Noise sensitivity analysis of the novel EKF operated at 500 rpm.

Noise level	Maximum absolute error	Steady state error
0%	0.48%	0.12%
1%	1.41%	0.2%
3%	1.81%	1.55%
5%	2.25%	1.61%

Table 6

Analysis of parameter variation for the novel EKF algorithm with PINN tested at 500 rpm.

Condition	Variation	Parameters	Maximum absolute error	Steady state error
L_s and K_e are fixed and R_s is varied	-20%	$R_s = 0.4\ \Omega$	0.37%	0.14%
	Nominal	$R_s = 0.5\ \Omega$	0.48%	0.12%
	+20%	$R_s = 0.6\ \Omega$	0.69%	0.15%
R_s and K_e are fixed and L_s is varied	-20%	$L_s = 0.0008$ H	0.52%	0.15%
	Nominal	$L_s = 0.0010$ H	0.48%	0.12%
	+20%	$L_s = 0.0012$ H	0.71%	0.16%
R_s and L_s are fixed and K_e is varied	-20%	$K_e = 0.8$	0.33%	0.14%
	Nominal	$K_e = 1$	0.48%	0.12%
	+20%	$K_e = 1.2$	0.59%	0.15%

Table 7

Acceleration and deceleration ramp test for the conventional and novel EKF algorithms.

Condition	Maximum absolute tracking error		Final tracking error	
	Acceleration	Deceleration	Acceleration	Deceleration
Terminal voltage sensing	49.38%	48.09%	0.11%	0.03%
Back-EMF	43.26%	41.97%	0.56%	0.3%
Conventional EKF	37.9%	34.8%	8.3%	6.12%
Novel EKF	26.2%	25.7%	6.25%	5.82%

Table 8

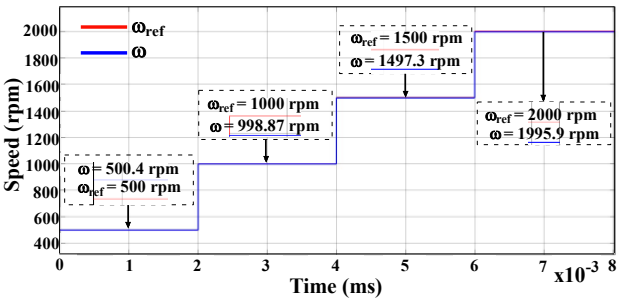
Speed reversal test for the conventional and novel EKF algorithms.

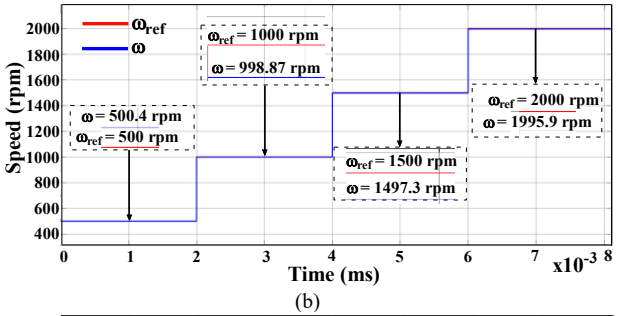
Reference speed	Positive speed tracking error	Negative speed tracking error
Terminal voltage sensing algorithm	21.52%	18.2%
Back-EMF algorithm	15.24%	14.87%
Conventional EKF algorithm	12.46%	10.75%
Novel EKF algorithm with machine learning based PINN algorithm	4%	3.3%

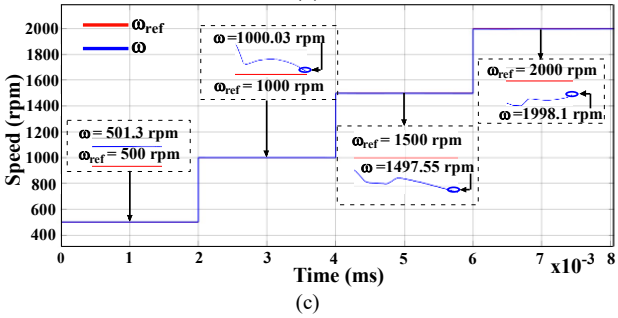
Table 9

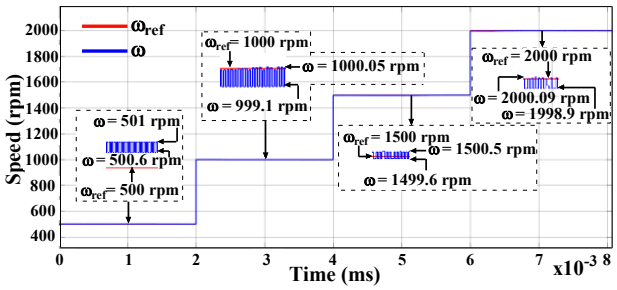
Comparison of the computational time of the conventional algorithm with the novel EKF algorithm with PINN tested at 500 rpm.

Algorithm	Computational time
Terminal voltage sensing algorithm	7552 ns
Back-EMF algorithm	8951 ns
Conventional EKF algorithm	5385 ns
Novel EKF algorithm with machine learning-based PINN algorithm	2805 ns









(d)

Fig. 7 – Experimental results of BLDC motor operating from 500 rpm to 2000 rpm for (a) Terminal voltage sensing algorithm (b) Back-EMF algorithm (c) Conventional EKF algorithm (d) Novel EKF algorithm with machine learning-based PINN algorithm.

5. CONCLUSION

A novel EKF is introduced for sensorless speed estimation of BLDC motors to achieve wider speed operating conditions, shorter computational time, and eliminate parameter variation issues. To achieve this, the initial speed is produced by igniting the motor in open-loop mode and then transformed to brushless mode, overcoming the low-speed estimation drawbacks. The machine learning-based PINN algorithm confirms the effectiveness of the implemented technique by tracking the estimated motor speed close to the reference speed. The implemented method is compared with conventional speed estimation techniques like the terminal voltage sensing algorithm, the back-EMF algorithm, and the EKF. Finally, experimental results confirm that the implemented speed estimation scheme has better speed estimation performance. The distinct advantages of the novel EKF with PINN are

1. Capable of embedding BLDC motor physics directly into a data-driven neural network algorithm.
2. Employing the novel EKF and PINN has the advantage of stability and faster convergence of the novel EKF with non-linear modeling and robust parameter learning capability of the PINN algorithm.

CREDIT AUTHORSHIP CONTRIBUTION STATEMENT

Priyanka SASIDHARAN: conceptualization, methodology, analysis, writing, and final approval of the manuscript.

Sriranjani RAMAKRISHNAN: conceptualization, methodology, analysis, writing, and final approval of the manuscript.

Jayalalitha SUBBAIAH: conceptualization, methodology, analysis, writing, and final approval of the manuscript.

Received on 2 March 2026

REFERENCES

1. H.M. CheshmehBeigi, “Design and implementation of the new sensorless rotor position estimation in homopolar salient-pole brushless DC motor,” IEEE J. Emerg. Sel. Top. Power Electron., **10**, *2*, pp. 2020–2029 (2022).
2. J.C. Gamazo-Real, V. Martínez-Martínez, J. Gomez-Gil, “ANN-based position and speed sensorless estimation for BLDC motors,” Measurement, **188**, article 110602 (2022).
3. C.L. Huang, C.J. Wu, S.C. Yang, “Full-region sensorless BLDC drive for permanent magnet motor using pulse amplitude modulation with DC current sensing,” IEEE Trans. Ind. Electron., **68**, *11*, pp. 11234–11244 (2021).
4. L. Yang, Z.Q. Zhu, H. Bin, Z. Zhang, L. Gong, “Virtual third harmonic back-EMF-based sensorless drive for high-speed BLDC motors considering machine parameter asymmetries,” IEEE Trans. Ind. Appl., **57**, *1*, pp. 306–315 (2021).
5. B. Saha, B. Singh, A. Sen, “SMO-based position sensorless BLDC motor drive employing canonical switching cell converter for light electric vehicle,” IEEE Trans. Ind. Appl., **59**, *3*, pp. 2974–2984 (2023).
6. S. Ok, Z. Xu, D.H. Lee, “A sensorless speed control of high-speed BLDC motor using variable slope SMO,” IEEE Trans. Ind. Appl., **60**, *2*, pp. 3221–3228 (2024).
7. D. Joshi, D. Deb, A.K. Giri, M. Elsisi, “Sensorless active disturbance rejection hybrid control with adaptive sliding mode observer for BLDC motor drives,” IEEE Trans. Power Electron., **40**, *12*, pp. 17832–17843 (2025).
8. J. De Viaene, D. Ceulemans, S. Derammelaere, K. Stockman, “Sensorless load angle control for energy-optimal sinusoidal-driven BLDC motor applications,” IEEE/ASME Trans. Mechatronics, **27**, *4*, pp. 2290–2300 (2022).
9. B. Saha, B. Singh, “Adaptive delay signal cancellation-synchronous reference frame phase-locked loop-based position sensorless single-stage BLDC motor drive for light-duty electric vehicle,” IEEE Trans. Ind. Appl., **60**, *2*, pp. 3229–3236 (2024).
10. B. Saha, B. Singh, “Sensorless BLDCM drive using an improved DSOGIPLL observer for solar-PV assisted LEV,” IEEE Trans. Power Electron., **40**, *1*, pp. 1636–1644 (2025).
11. M. Akrami, E. Jamshidpour, B. Nahid-Mobarakeh, S. Pierfederici, V. Frick, “Sensorless control methods for BLDC motor drives: A review,” IEEE Trans. Transp. Electrific., **11**, *1*, pp. 135–152 (2025).
12. P. Ramesh, A. Ranjeev, C. Santhakumar, J. Vinothand, C. Bharatiraja, “Sensor-less field orientation control for brushless direct current motor controller for electric vehicles,” Mater. Today: Proc., **65**, pp. 277–284 (2022).
13. R. İnan, B. Aksoy, O.K.M. Salman, “Estimation performance of the novel hybrid estimator based on machine learning and extended Kalman filter proposed for speed-sensorless direct torque control of brushless direct current motor,” Eng. Appl. Artif. Intell., **126**, article 107083 (2023).
14. P. Kumar, D.V. Bhaskar, U.R. Muduli, A.R. Beig, R.K. Behera, “Iron-loss modeling with sensorless predictive control of PMBLDC motor drive for electric vehicle application,” IEEE Trans. Transp. Electrific., **7**, *3*, pp. 1506–1515 (2021).
15. A. Sen, B. Singh, “Parametric observer-controlled motor-invariant electronic commutation of photovoltaic-powered BLDCM without position sensor,” IEEE Trans. Power Electron., **38**, *9*, pp. 11304–11314 (2023).
16. B. Saha, B. Singh, A. Sen, “Solar PV integration to e-rickshaw with regenerative braking and sensorless control,” IEEE Trans. Ind. Appl., **58**, *6*, pp. 7680–7691 (2022).
17. A. Derbane, B. Tabbache, A. Ahrichea, “Fuzzy logic approach based direct torque control and five-leg voltage source inverter for electric vehicle powertrain,” Rev. Roum. Sci. Techn. – Électrotechn. Et Énerg., **66**, *1*, pp. 15–20 (2021).
18. H. Lallouani, O. Moussa, A. Bouzidi, A. Akka, “Interval type-2 fuzzy logic control for brushless doubly fed induction generator based on wind energy conversion systems,” Rev. Roum. Sci. Techn. – Électrotechn. Et Énerg., **70**, *3*, pp. 307–311 (2025).
19. L. Popescu, O. Craiu, “Energy consumption analysis for an EV powertrain using three BLDC identical motors,” Rev. Roum. Sci. Techn. – Électrotechn. Et Énerg., **68**, *2*, pp. 152–157 (2023).
20. S.E. Chouaba, A. Barakat, “Dynamic de-excitation performance of brushless synchronous machines using advanced control strategy,” Rev. Roum. Sci. Techn. – Électrotechn. Et Énerg., **70**, *4*, pp. 501–506 (2025).
21. M. Kavya, S. Jayalalitha, “A novel shift and search (S&S) algorithm for tracking maximum power in PV systems: An approach to increase efficiency,” Int. J. Precis. Eng. Manuf.-Green Technol., **8**, *6*, pp. 1699–1710 (2021).
22. R.M. Paruthipulli Kalarikkal, S. Jayalalitha, “Modified dual EKF with machine learning model for fouling prediction of industrial heat exchanger,” Korean J. Chem. Eng., **41**, *4*, pp. 1013–1027 (2024).
23. R. Sriranjani, S. Jayalalitha, “Hardware-in-the-loop cosimulation of LMS algorithm for shunt active filter to mitigate harmonics and reactive power—Xilinx System Generator approach,” J. Control Eng. Appl. Inform., **21**, *4*, pp. 71–7 (2019), https://www.ceai.srait.ro/index.php/ceai/issue/view/321